Odor coding by modules of coherent mitral/tufted cells in the vertebrate olfactory bulb

Tsai-Wen Chen[a,b,c,1], Bei-Jung Lin[b,d,1], and Detlev Schild[a,b,c,d,2]

[a]DFG Research Center for Molecular Physiology of the Brain, [b]Bernstein Center for Computational Neuroscience, [c]Institute of Physiology, and [d]DFG Cluster of Excellence, University of Göttingen, Göttingen, Germany

Edited by Randall R. Reed, Johns Hopkins University School of Medicine, Baltimore, MD, and accepted by the Editorial Board December 8, 2008 (received for review October 13, 2008)

Odor representation in the olfactory bulb (OB) undergoes a transformation from a combinatorial glomerular map to a distributed mitral/tufted (M/T) cell code. To understand this transformation, we analyzed the odor representation in large populations of individual M/T cells in the *Xenopus* OB. The spontaneous [Ca^{2+}] activities of M/T cells appeared to be irregular, but there were groups of spatially distributed neurons showing synchronized [Ca^{2+}] activities. These neurons were always connected to the same glomerulus. Odorants elicited complex spatiotemporal response patterns in M/T cells where nearby neurons generally showed little correlation. But the responses of neurons connected to the same glomerulus were virtually identical, irrespective of whether the responses were excitatory or inhibitory, and independent of the distance between them. Synchronous neurons received correlated EPSCs and were coupled by electrical conductances that could account for the correlated responses. Thus, at the output stage of the OB, odors are represented by modules of distributed and synchronous M/T cells associated with the same glomeruli. This allows for parallel input to higher brain centers.

calcium imaging | mitral cell | synchronous activity

The glomeruli of the olfactory bulb (OB) constitute an important interface for the coding of odor information. Every individual glomerulus collects convergent inputs from olfactory sensory neurons (OSN) expressing the same olfactory receptor (OR) (1), and it delivers output information to higher brain regions via a number of M/T cells connected to it (2). This modular architecture is thought to play a fundamental role in odor coding (3).

M/T cells of the same glomerulus receive primary inputs from OSNs of the same type, but each M/T cell also extends additional dendrites and gets complex secondary inputs from local interneurons (4, 5), top-down projections (6, 7), and from other M/T cells (8, 9). M/T cells are also connected through gap junctions within glomeruli (9–11). While the intraglomerular gap junctions could produce a certain degree of synchronization (9, 11, 12), the synaptic interactions could transform the initial OSN inputs into spatiotemporal patterns of M/T cell output activity (13–15). As the secondary inputs presumably differ from M/T cell to M/T cell, every M/T cell could process its primary and secondary inputs differentially, which would allow for a large information capacity of M/T cell activity patterns.

Three major signal sources thus determine the M/T cell activity patterns conveyed to higher brain centers: primary OSN inputs, currents through intraglomerular gap junctions, and complex secondary synaptic inputs of various origins. As all three input sources of M/T cells depend, directly or indirectly, on odor stimulation, the physiological M/T cell activity patterns must be measured while applying odorants to the olfactory epithelium.

Here, we use a nose-brain preparation of the *Xenopus* tadpole to analyze M/T cell activity pattern following natural odor stimulation. Using a method for identifying neurons that are connected to the same glomerulus, we can observe how natural odorants are represented by modules of glomerulus-specific M/T cells.

Results

Identification of Glomerulus-specific M/T Cells Using [Ca^{2+}] Imaging. We investigated the neuronal network of the *Xenopus* tadpole OB using a combination of [Ca^{2+}] imaging and the patch clamp technique. Recordings were obtained from a nose-brain preparation that preserves the connections between the olfactory epithelium and the OB (16, 17) (Fig. S1). This allows us to analyze the circuitry and the response of the OB network to natural odor inputs. In the absence of stimulation, neurons in the M/T cell layer show a rich pattern of spontaneous [Ca^{2+}] activities (Fig. 1*A* and *B*) that reflect their spontaneous firing patterns (Fig. S2) (18). The correlation of these activities was low in randomly chosen cell pairs (activity correlation index $r = 0.0069 \pm 0.0003$; $n = 50325$ pairs). However, a complete search in a correlation matrix (Fig. 1*C*) revealed specific pairs of neurons that showed strongly correlated activities ($r > 0.6$, Fig. 1*D*, *E*, and *G*). These neurons were synchronized for almost every [Ca^{2+}] upstroke (Fig. 1*D* and Movie S1). Correlated activities in synchronous neurons were stable over time. The same pair of neurons remained synchronous in different recording sessions spanning more than an hour.

Synchronous neurons were distributed in the M/T cell layer and were intermixed with cells belonging to other synchronous modules (Fig. 1*F*). The distance between synchronous neurons ranged from 10 to 184 μm (Fig. 1*H*, average: 53 ± 37 μm, SD; $n = 73$ pairs). A neuron could be uncorrelated with its immediate neighbor (e.g., cells 6 and 8, $r = 0.09$) while at the same time being tightly correlated with a more distant cell (e.g., cells 6 and 7, $r = 0.78$). We often found more than two neurons in the recorded field of view that were synchronous with each other (e.g., cells 1–3 in Fig. 1*F*). The number of neurons making up a synchronous group ranged from 2–7 cells, the average being 2.4 cells/group. This average underestimates the total number of cells per synchronous group because some neurons of a group might have been located outside the image plane and not been detected. Synchronous neurons were found both in preparations with intact olfactory nerves (3.8 ± 1.0 pairs/optical section, $n = 19$) as well as in preparations with the olfactory nerves cut (4.6 ± 1.4 pairs/optical section, $n = 16$; $P > 0.66$; Fig. S3), suggesting that the coordinated activity was intrinsic to the OB and did not require OSN inputs.

To analyze the correlated spiking at a higher temporal resolution, we recorded the action potentials (AP) of cell pairs using dual cell-attached recordings. Without any stimulation, M/T cells fired spontaneous APs that were highly correlated in cell pairs showing synchronous [Ca^{2+}] activities (Fig. 1*I*). The cor-

Author contributions: T.-W.C., B.-J.L., and D.S. designed research; T.-W.C. and B.-J.L. performed research; T.-W.C. and B.-J.L. analyzed data; and T.-W.C., B.-J.L., and D.S. wrote the paper.

The authors declare no conflict of interest.

This article is a PNAS Direct Submission. R.R.R. is a guest editor invited by the Editorial Board.

[1]T.-W.C. and B.-J.L. contributed equally to this work.

[2]To whom correspondence should be addressed. E-mail: dschild@gwdg.de.

This article contains supporting information online at www.pnas.org/cgi/content/full/0810151106/DCSupplemental.

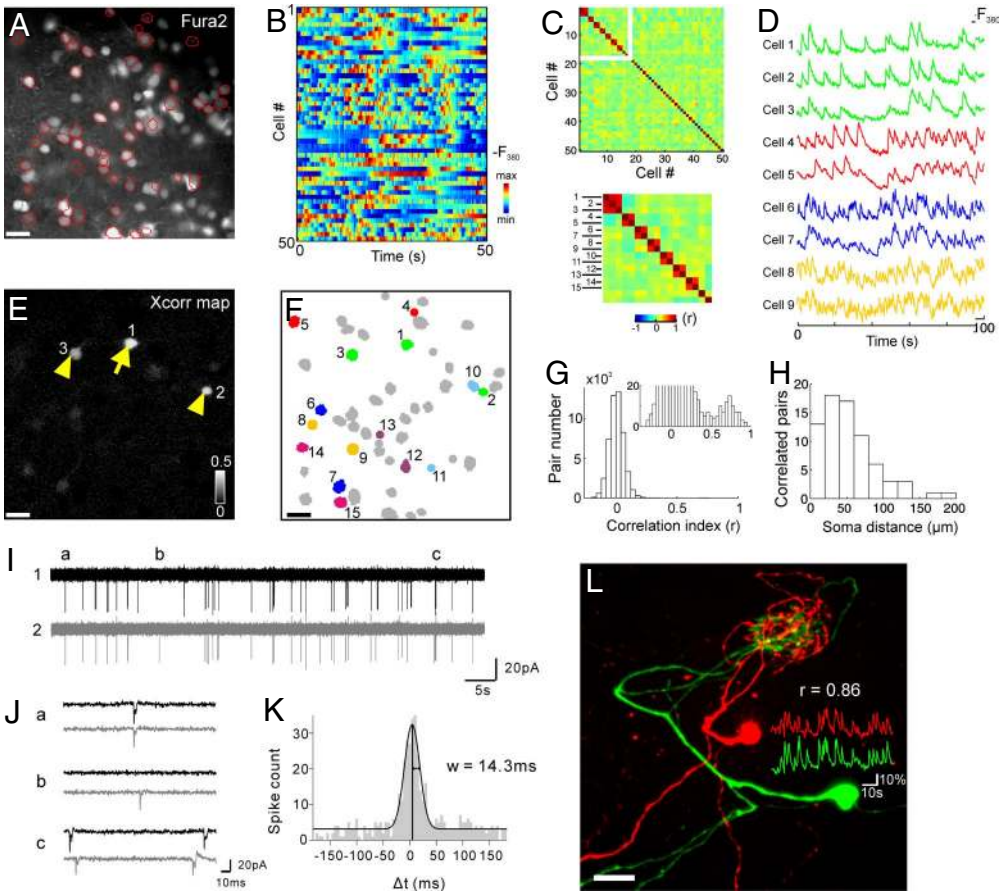

Fig. 1. Identification of connected M/T cells using cross-correlation analysis. (*A*) A fluorescence image of the M/T cell layer stained with calcium indicator Fura-2. (*B*) Spontaneous $[Ca^{2+}]$ signals of 50 simultaneously recorded cells. (*C*) A correlation matrix of calcium signals in the 50 neurons. Cells are rearranged according to the correlation values. Distinct regions of high correlation coefficients reveal groups of synchronous neurons. (*D*) $[Ca^{2+}]$ signals in 4 groups of synchronous neurons. (*E*) A pixel-based map of cross-correlation values calculated with respect to the activity of the neuron marked by an arrow. Two cells (arrowheads) were synchronous to the reference cell. (*F*) Cells belonging to different synchronous groups marked by different colors. (*G*) Histogram of the correlation values of 50,325 cell pairs. Inset, a peak in the high correlation range showing the presence of synchronous pairs. A similar peak does not exist in the negative correlation range ($r<-0.5$). (*H*) Histogram of the distances between synchronous cell pairs ($r > 0.6$, $n = 73$ pairs). (*I*) Simultaneous on-cell recording of action potentials in a pair of synchronous neurons. (*J*) Expanded traces from regions marked in I. (*K*) Spike cross-correlogram showing the distribution of the lag (Δt) in spike time between the two cells. (*L*) Morphological reconstruction of a pair of synchronous neurons revealed their dendritic connections to the same glomerulus. (Scale bars, 20 μm.)

related spikes did not have a fixed delay. The two neurons could either fire nearly simultaneously or with a small positive or negative time lag (Δt) (Fig. 1*J*). The distribution of Δt showed a narrow peak near $\Delta t = 0$ (Fig. 1*K*), indicating that spikes of one neuron tended to occur within a narrow time window around the spikes of the other neuron and vice versa. A Gaussian fit to the distribution peaked, on the average, at 4.2 ± 1.0 ms ($n = 5$) with a standard deviation of the fitted curves of 14.9 ± 3.0 ms ($n = 5$). These results show that the synchronous neurons fire correlated APs at a precision of a few milliseconds.

A tight synchronization of both $[Ca^{2+}]$ and spiking activities is highly suggestive of some connection between synchronous neurons. To test this possibility, we reconstructed the morphology of nine pairs of synchronous cells ($r > 0.6$) by filling them with fluorescent tracers during targeted whole-cell recording. All 18 cells had dendrites that extended into the glomerular layer and terminated in tuft-like structures, confirming their identity as M/T cells. In all cell pairs examined, the two synchronous neurons invariably had dendrites that connected to the same glomerulus (Fig. 1*L* and Movie S2). In contrast, nearby but nonsynchronous neurons ($r < 0.4$) projected their dendrites into different glomeruli ($n = 3$ pairs). The soma distances of the synchronous pairs examined ranged from 20–109 μm (average: 57.3 μm). This indicates that synchronous M/T cells, irrespective of the distance between their somata, are output elements of the same glomerulus.

Responses of Synchronous Neurons to Natural Odor Simulations. The reliable relationship between the synchronization of spontaneous $[Ca^{2+}]$ activities and common glomerular connection offers a highly specific criterion for identifying glomerulus-specific neurons online. This enabled us to analyze how odors are represented by M/T cells that diverge from the same glomerulus. To this end, we first recorded spontaneous $[Ca^{2+}]$ activity of M/T cells to infer their glomerular connectivity and then recorded their odorant responses.

Generally, odor stimulation modulated the activities of M/T cells in at least two different ways (Fig. S4) (18). In some cells, odors reliably induced $[Ca^{2+}]$ increases that could be clearly distinguished from their spontaneous activities. In other cells, odor suppressed spontaneous $[Ca^{2+}]$ transients, leading to a $[Ca^{2+}]$ decrease with respect to the pre-stimulus level (Fig. S4). We quantified the responses of 448 cells (nine bulbs) to an odorant stimulus (mixture of 14 amino acids, see Materials and Methods). An excitatory or inhibitory response was assumed when the fluorescence change within a 7-s post-stimulus window exceeded $\pm$ 2.5 SD of the spontaneous fluctuations. Using this criterion, 29.5% of the examined neurons showed excitatory responses and 14.7% showed inhibitory responses.

The spatial distribution of odor-responsive M/T cells was highly heterogeneous (Fig. S4). There was a substantial intermix of neurons that showed excitatory responses with others showing inhibitory responses. In 177 randomly chosen pairs of neighboring and odor-responsive neurons, 57 pairs responded in an opposite way (i.e., excitation in one cell and inhibition in the other one). In cases where both responses were either excitatory or inhibitory, their durations or response waveforms would differ (Fig. S4).

Despite this marked variety of different response patterns of OB neurons, we observed a striking response similarity in synchronous neurons. Whenever an odor elicited an excitatory response in one neuron, its synchronous partner also responded with excitation (Fig. 2*A*, left). This is consistent with the synchronous neurons sharing common excitatory OSN inputs within the same glomerulus (1). To our surprise, when odor elicited inhibitory responses in one neuron, its synchronous partner also responded with inhibition (Fig. 2*A*, right). Such highly similar excitatory or

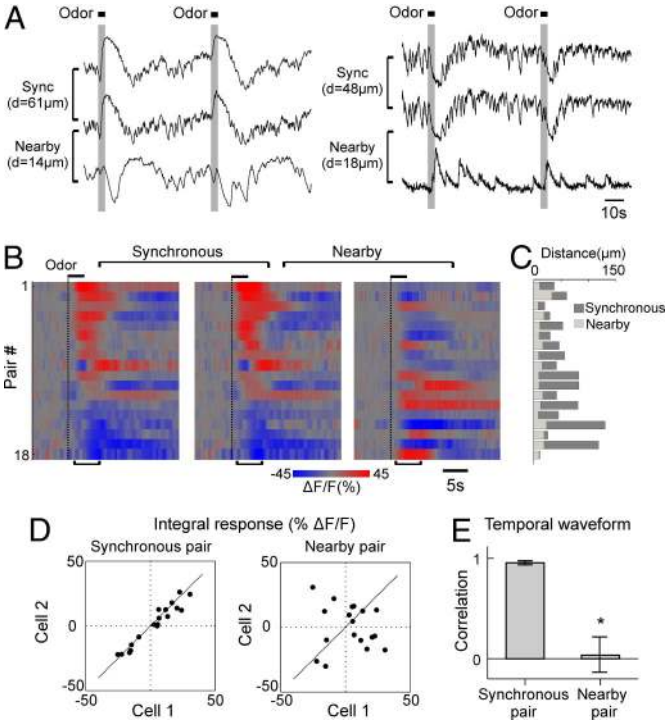

Fig. 2. Synchronous M/T neurons show precisely matched excitatory/inhibitory odor responses. (*A*) Odor modulation of $[Ca^{2+}]$ signals in two pairs of synchronous M/T neurons. The first pair consistently responds with an increase in $[Ca^{2+}]$ (left) while the second pair responds to the same odor with a $[Ca^{2+}]$ decrease (right). Bottom traces: The response of a nearby, nonsynchronous neuron. (*B*) Odor-induced calcium responses color coded and shown for 18 pairs of synchronous M/T cells (left and middle panel). The responses of nonsynchronous neurons located next to one of the synchronous cells as a control (right panel). (*C*) The soma distances between the synchronous pairs and the nearby pairs in (*B*). (*D*) Integral responses in a poststimulus time window (marked under the panels in B) plotted for the synchronous cell pairs (left) and the nearby, nonsynchronous pairs (right). (*E*) The correlation coefficient of the response waveforms in synchronous pairs and nearby pairs ($n = 18$; *, $P < 10^{-4}$).

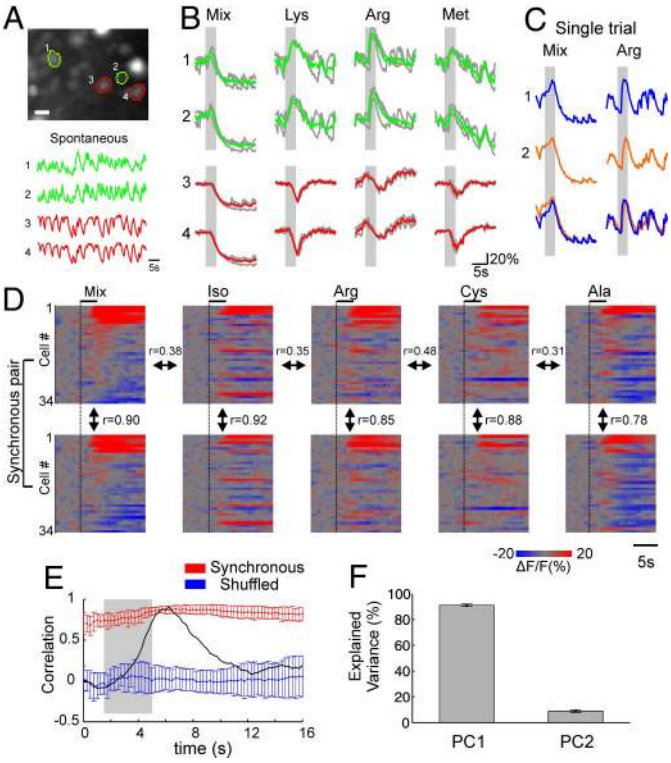

Fig. 3. Two copies of odor codes in the *Xenopus* OB. (*A*) Two pairs of synchronous M/T cells (top) and their spontaneous $[Ca^{2+}]$ signals (bottom). Scale bar, 10 μm. (*B*) The responses of the four neurons to four different odorants (amino acid mixture, lysine, arginine and methionine, 50 μM). Color traces show average responses, gray traces show individual trials. (*C*) Single trial responses of a synchronous pair and their overlay. (*D*) Responses of 34 neurons to five odors (upper row). The same odors are similarly represented by the synchronous partners of these neurons (lower row). r, correlation coefficient. (*E*) The correlation coefficient (r) between the two ensembles measured in successive 250-ms windows plotted over time (red). Re-shuffling the cell order eliminates the correlation (blue). Error bars represents the SEM of r values over 12 trials (6 odors, each applied twice). Black trace shows the response waveform averaged over all neurons. (*F*) Percentage of response variance covered by the first (PC1) and the second principle component (PC2). Using a single variable (PC1) explains >90% of the variance of the responses of synchronous neurons.

inhibitory responses were observed in all 18 pairs of synchronous neurons (Fig. 2*B*). The strong similarity of odor responses was restricted to synchronous neurons. A neuron can show substantially different or even opposite responses to its nearest, nonsynchronous neighbor but always show a precisely matched response to a synchronous, although more distant, neuron (Fig. 2*A* and *B*). The responses of the synchronous neurons were similar not just in direction but also in amplitude, duration and temporal patterns (Fig. 2*B*). We quantified the amplitudes and the response waveforms in 18 pairs of synchronous neurons and in 18 nonsynchronous neurons located next to one of the synchronous neurons. Although the synchronous neurons were separated by larger distances (Fig. 2*C*), their responses, in particular the response directions, amplitudes (Fig. 2*D*) and the temporal waveforms (Fig. 2*E*) were more similar than in nearby, nonsynchronous pairs.

The response similarity of synchronous neurons was not limited to a particular odorant. When applying different odorants to the olfactory epithelium, we observed different odor-specific response patterns (Fig. 3*B*), indicating that these neurons carried information about odor identity. In nearby nonsynchronous neurons (e.g., cells 2 and 3 in Fig. 3*A* and *B*), the responses were similar for some odorants (e.g., the amino acid mixture inhibited both cells 2 and 3) but different for others (e.g., lysine excited cell 2 but inhibited cell 3). However, in neurons belonging to the same synchronous module, different odorants led to virtually identical responses (Fig. 3*B* and *C*).

Fig. 3*D* shows an ensemble representation of five different odors by 34 M/T neurons (Fig. 3*D*, upper row). Each odor was represented by a specific pattern of excitation/inhibition distributed across the population. In the ensemble formed by the synchronous partners of these neurons (Fig. 3*D*, lower row), we observed highly similar representations of the same odors ($r = 0.87 \pm 0.02$; $n = 5$ odors). The high correlation was not due to a lack of specificity of the $[Ca^{2+}]$ response waveforms because random reshuffling of the cell indices eliminated the correlation (r shuffled $= 0.03 \pm 0.01$). Further, when the correlation was measured over short time windows (250 ms), the correlation was reliable before, during and after odor responses (Fig. 3*E*). The high correlation suggests that synchronous neurons essentially carry the same odorant feature. This is confirmed by principal component analysis, which shows that the first principle component explains >90% of the variance of the cell pairs' odor responses ($91.1 \pm 0.9\%$, $n = 34$ pairs, Fig. 3*F*). Thus, higher brain centers could retrieve virtually the same odor information using both or either of the synchronous neurons.

We further recorded the odor modulation of spiking activities in pairs of synchronous neurons using dual patch clamp. Consistent with imaging data, odors can modulate the spiking of M/T cells in excitatory or inhibitory direction. In synchronous neurons, both the

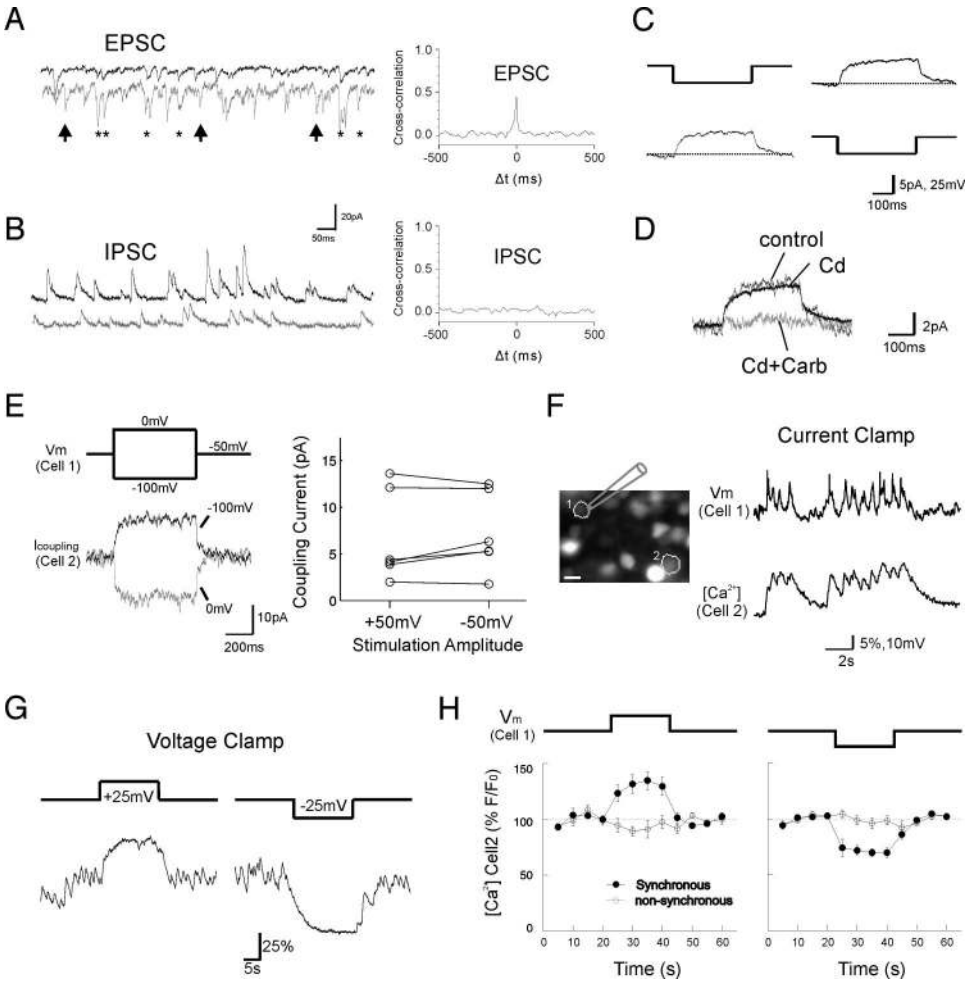

Fig. 4. Mechanism of correlated activities in synchronous M/T cells. (*A*) Left, excitatory synaptic currents (EPSC) in a pair of synchronous neurons measured at −60 mV. Asterisks: synchronous events; arrows: asynchronous events. Right, membrane current cross-correlogram had a peak ($r = 0.43$) near $\Delta t = 0$. (*B*) Left, inhibitory synaptic currents (IPSC) in synchronous neurons measured at 0 mV. Most IPSC events are not synchronous. Right, cross-correlogram of the IPSCs do not show a significant peak. (*C*) Hyperpolarizing voltage steps (−60 to −85 mV) in one M/T cell elicit hyperpolarizing (outward) currents in its synchronous partner (left column) and vice versa (right column). The current traces are averages of 80 sweeps. (*D*) The coupling current is not affected by Cd^{2+} but it is abolished by subsequent application of gap junction inhibitor carbenoxolone (Carb). (*E*) Application of depolarizing or hyperpolarizing pulses to one neuron (upper) elicited nearly symmetrical coupling current responses in its synchronous partner (lower). Right: summary of coupling current responses in 4 pairs of synchronous neurons (6 coupling directions) (*F*) Simultaneous recording of membrane potential in a mitral cell (cell 1) during spontaneous $[Ca^{2+}]$ activity of its synchronous partner (cell 2). The voltage in cell 1 is locked to the $[Ca^{2+}]$ activity of cell 2. (*G*) Stimulating a patch-clamped neuron in depolarizing or hyperpoloarizing direction specifically enhances or suppresses the $[Ca^{2+}]$ activity of its synchronous partner. (*H*) Summary (mean ± SEM.) of the $[Ca^{2+}]$ activity modulation in synchronous ($n = 4$) and nonsynchronous ($n = 7$) pairs.

excitatory/inhibitory spiking responses were highly similar (Fig. S5). The tuning curves reconstructed by measuring the changes in firing rate across 6 odors had similar shapes in synchronous neurons (Fig. S5; $n = 4$ pairs). These data suggest that downstream neurons can rely on correlated odor responses of synchronous neurons.

Mechanisms of Correlated Activity in Synchronous M/T Cells. How can the neurons of a synchronous module show such highly coordinated ongoing, odor-modulated activities? In other systems, correlated neuronal activities have been attributed to common excitatory inputs (19), synchronous inhibitory inputs (20, 21) or a direct coupling among neurons (11, 22). We investigated these possibilities by recording pairs of synchronous neurons using dual whole-cell patch clamp. At −60mV, M/T cells predominantly showed synaptic inward currents that could be blocked by CNQX and APV. In synchronous neurons, some of these EPSC events occurred concurrently in both cells (Fig. 4*A*, asterisks) while others occurred in only one of the neurons (arrows). The cross-correlogram of the membrane currents had a peak near $\Delta t = 0$ [$r(0) = 0.35 \pm 0.07$; $n = 8$], suggesting that the excitatory inputs of these neurons exhibit a certain degree of correlation. At a potential close to the reversal potential for ionotropic currents mediated by glutamate receptors (0 mV), M/T cells predominantly showed synaptic outward currents that were abolished by picrotoxin (50 μM). Examining these currents revealed that the IPSC events rarely occurred simultaneously in synchronous neurons (Fig. 4*B*). The cross-correlogram of the membrane currents did not show a detectable peak [$r(0) = 0.05 \pm 0.02$; $n = 4$]. As a control, we recorded the spontaneous synaptic currents in nonsynchronous M/T cell pairs. Here, both EPSCs and IPSCs were essentially uncorrelated. The cross-correlograms of EPSCs and IPSCs did not show any peak near $\Delta t = 0$ [$r(0) = 0.001 \pm 0.002$ for EPSP and 0.004 ± 0.01 for IPSC, $n = 3$ pairs, see Fig. S6]. Taken together, these data suggest that synchronous cell pairs receive correlated excitatory input, and that IPSCs play a relatively minor role in synchronizing the spontaneous activity of M/T cells.

We next examined the possibility of a direct coupling between synchronous M/T cells. Studies in the mammalian OB show that M/T cells connected to the same glomerulus are coupled by gap junctions (9, 11, 23). Because gap junctions can pass both depolarizing and hyperpolarizing currents, they could play a role in coordinating the excitatory/inhibitory responses. In whole-cell recordings that specifically targeted synchronous M/T cells, a 25 mV hyperpolarization pulse (from −60 to −85 mV) applied to one cell (cell 1) reliably elicited a hyperpolarizing (outward) current in its synchronous partner (cell 2, averaged amplitude: 3.73 ± 0.51 pA; $n = 10$ pairs, Fig. 4*C*). A current of similar amplitude was observed in cell 1 when the voltage pulses were applied to cell 2 (Fig. 4*C*, right). Also, depolarizing and hyperpolarizing voltage steps in one cell resulted in currents of opposite sign but similar amplitude in the other cell (Fig. 4*E*). The coupling current was not seen in recordings made in pairs of nearby nonsynchronous neurons ($n = 3$, data not shown), suggesting that the coupling was specific for synchronous cells. Finally, Cd^{2+} (200 μM), which blocked most synaptic currents, had little effect on the coupling current whereas the gap junction inhibitor carbenoxolone (200–400 μM) largely reduced the current (Fig. 4*D*, 80 ± 11% reduction, $n = 4$). These results show that the synchronous M/T cells in the *Xenopus* OB are electrically coupled,

suggesting that a glomerulus-specific M/T cell coupling is a general feature of glomerular function in the vertebrate OB.

Because *Xenopus* M/T cells have large input resistances (>1GΩ) (24), the electrical coupling conductances we observed could have a strong effect. We tested this by patch clamping one M/T cell (cell 1) while simultaneously monitoring the $[Ca^{2+}]$ activity of its synchronous partner (cell 2). Consistent with a role of electrical coupling in synchronizing M/T cell activity, we observed a potential in cell 1 coupled to the spontaneous $[Ca^{2+}]$ signals in cell 2 (Fig. 4*F*). To test whether the coupling could be strong enough to coordinate odor-induced responses, we stimulated the patch clamped neuron while measuring the $[Ca^{2+}]$ activities of other neurons. In these experiments, depolarizing a single M/T cell induced measurable excitatory $[Ca^{2+}]$ responses in its synchronous partner (but not in other cells in the same field of view, Fig. 4*G* and *H*, $n = 4$ synchronous pairs and 7 nonsynchronous pairs). Moreover, hyperpolarizing the neuron reduced the spontaneous activities of its synchronous partner (Fig. 4*G* and *H*), leading to a $[Ca^{2+}]$ decrease similar to inhibitory odor-induced $[Ca^{2+}]$ responses (Fig. 2*A*, right). These data show that depolarizing or hyperpolarizing an M/T cell can propagate and specifically modulate the responses of other synchronous neurons. This provides a mechanism to coordinate the responses of synchronous neurons during odor processing in the OB.

Discussion

Correlated Spontaneous Activity of M/T Cells and Their Potential Functions. By analyzing correlated $[Ca^{2+}]$ activities of OB neurons, we have been able to specifically identify connected M/T cells in living tissue (Fig. 1). This characterizes their functional coupling (Fig. 4) and reveals a precise relationship between the odor representation of M/T cells and their glomerular connectivity (Figs. 2 and 3). A tight correlation of spiking discharges has long been used as an indication of connections between neurons (9, 25, 26). However, finding connected pairs in living tissue remains a challenging task because of a low connection probability in most networks and the technical difficulty to simultaneously record from many cell pairs. Using $[Ca^{2+}]$ imaging, we can easily test the correlated activities in thousands of cell pairs in a single experiment, allowing us to identify connected M/T cell pairs in almost every preparation. This approach might be generally useful for identifying connected neurons in other neuronal networks.

In addition to its use as an experimental tool, the correlated spontaneous activity might serve specific functions. For example, as M/T cells connected to the same glomerulus can be identified from their synchronous ongoing activities, they could provide a tonic 'identity signal' to downstream neuronal circuits for inferring the common glomerular specificity of incoming axons without requiring odorant exposure. This may be important for the establishment of specific circuit connections in higher olfactory centers. In addition, correlated activities of M/T cells could play a role for the insertion of newborn granule cells, which continuously migrate into the OB and have to make specific connections with M/T cells (27).

Mechanism of Correlated Activity. The data from paired recordings reveal correlated EPSCs and noncorrelated IPSCs in synchronous neurons. The simplest explanation for correlated EPSCs is a common input from OSNs. As the dendritic fields of synchronous neurons overlap extensively within the glomerulus (Fig. 1*L* and Movie S2), these neurons could be simultaneously contacted by the same OSNs. Activation of these OSNs would lead to correlated EPSCs. On the other hand, at 0 mV, the IPSC events in synchronous neurons show virtually no correlation (Fig. 4*B*). This suggests that IPSCs play a relatively minor role in synchronizing the spontaneous activity of M/T cells. These data, however, do not exclude the role of inhibitory networks in coordinating stimulus-induced M/T cell activity. For example, a synchronous activation of inhibitory neurons (e.g., by patterned ON stimulation) might lead to correlated IPSCs (21) and further enhance the correlated activity of M/T cells.

Previous studies in the mammalian OB revealed that mitral cells of the same glomerulus show ubiquitous gap junction coupling and an AMPA mediated coupling component in a subset of cells (10). Our data consistently showed gap junction currents in synchronous neurons of the *Xenopus* OB. The coupling conductance was 150 ± 20 pS (range:48–256 pS, $n = 10$ pairs), and the current was nearly symmetrical during application of ± 50mV stimulation pulses (Fig. 4*E*). Because + 50 mV voltage pulses are sufficient to open voltage gated calcium channels and induce neurotransmitter release, a symmetrical coupling current suggests that the coupling is presumably mostly electrical. As *Xenopus* M/T cells have small somata (≈10 μm diameter) and high input resistences (> 1 GΩ), the electrical coupling alone can already have a strong functional effect. This is illustrated by the experiment shown in Fig. 4*G* and *H*. In these experiments, a 25 mV de- or hyperpolarization in a single M/T cell induced $[Ca^{2+}]$ responses in its synchronous partner. This strong coupling could play an important role for the coordination of odor-induced responses.

The Response of Synchronous Neurons to Natural Odors. Recently, the correlation between M/T cells of the same glomerulus has been examined in slices of the rodent olfactory bulb (9, 11, 28, 29). Using paired recordings, these studies have revealed that neighboring M/T cells of the same glomerulus can exhibit correlated activity upon electrical or pharmacological stimulation (9, 11, 28, 29). However, the preparations used did not preserve the OSN inputs, and therefore could not show how synchronous neurons behaved during processing of natural odors. The odor response properties of M/T cells have been examined using both electrophysiology and imaging techniques *in vivo* (30–33) or using *in vitro* nose-brain preparations (14, 15, 18, 34). However, none of these studies related the odor response of M/T cells to their glomerular connectivity. It was thus impossible to make any assertion regarding a modular odor coding scheme as shown in the present study. Here we have analyzed the odor responses of M/T cells with respect to their common glomerular connection as inferred from their synchronous spontaneous activity. Our data show that M/T cell responses are highly similar in neurons connected to the same glomerulus during both odor-induced excitation and inhibition, while activities in neighboring cells are mostly uncorrelated.

One immediate implication of the highly correlated responses is that they largely reduce the number of potentially independent coding variables of the OB's output. Generally, to describe a neural system containing N neurons, one would need N variables each representing the activity of a neuron. Thus, the neural representation of each odor could be considered as a vector in an N-dimensional "coding space" (35), with N being the total number of M/T cells. However, our data suggest that the actual size of the OB's coding space is presumably much smaller than N. Indeed, more than 90% of the variance of synchronous M/T cell pair responses can be explained by one variable (Fig. 3*F*). Although it is presently not feasible to simultaneously record *all* M/T cells connected to the same glomerulus, the extrapolation of our findings suggests that the dimension of the OB's coding space might be close to the number of glomeruli.

The OB projects its outputs to the cortex and to other higher brain areas that mediate learning, memory and the emotional responses to odors (3). The OB as the interface between olfactory sensory neurons and central brain areas has to coordinate the odor information sent to various target areas. Recent studies have revealed that the axonal outputs of a given glomerulus target multiple locations in higher brain regions (36). A correlated response of these glomerulus-specific outputs appears to be consistent with such parallel distribution of odor information. Thus, individual glomeruli could be viewed not only as convergence centers of OSN inputs but also as the starting points of parallel

"broadcasting channels" that deliver coherent odor information to higher brain regions.

Materials and Methods

***Xenopus* Tadpole Nose-Brain Preparation.** *Xenopus laevis* tadpoles (stage 53–55) were chilled in a mixture of ice and water, and decapitated as approved by the Göttingen University Committee for Ethics in Animal Experimentation. A block of tissue containing the olfactory mucosae, intact olfactory nerves, and most of the brain (Fig. S1) was cut out and kept in physiological saline (in mM, NaCl 98, KCl 2, $CaCl_2$ 1, $MgCl_2$ 2, glucose 5, Na-pyruvate 5, and Hepes 10; 230 mOsm, pH 7.8). The dorsal part of the olfactory bulb was sliced off to expose neurons for imaging and patch-clamp recordings. The olfactory mucosae and nerves were kept intact unless stated otherwise.

Dye Loading and Calcium Imaging. To load the neurons with $[Ca^{2+}]$-sensitive dye, the preparations were incubated in a bath solution containing 50 μM of Fura-2/AM or Fluo-4/AM (Molecular Probes) for 30 min at room temperature, and then rinsed with bath solution for at least 30 min in the recording setup. $[Ca^{2+}]$ measurements with Fura-2 were performed using an upright microscope (Axioskop 2, Zeiss) with a 40× (NA = 0.8) objective. Fluorescence images excited at 380 nm were taken at 5 Hz using a frame-transfer, back-illuminated CCD camera (Micromax, Visitron). Confocal imaging with Fluo-4/AM was performed using a laser scanning microscope (Zeiss LSM 510/Axiovert 100M) with a 40× (NA = 1.3) oil immersion objective. Fluorescence images (excited at 488 nm) were acquired at 4 Hz.

Odorant Stimulation. A mixture of 14 L-amino acids (alanine, serine, threonine, cysteine, valine, leucine, isoleucine, methionine, proline, arginine, lysine, histidine, phenylalanine, and trytophan, 10 μM in Ringer's solution) or single amino acids (50–100 μM in Ringer's solution) were used as odorants. Short pulses (1 s) of odorant were applied by triggering odor delivery valves using custom build recording software. In experiments involving many odors (Fig. 3), repeated stimulations of an odor were interleaved with the application of other odorants.

Targeted Electrophysiological Recordings and Morphological Reconstructions. Imaging data were first analyzed online to select neurons showing synchronous activities. The same cells were then re-identified under transmission optics. Patch pipettes containing internal solution (in mM, NaCl 2, KCl 11, $MgSO_4$ 2, K-gluconate 80, Hepes 10, EGTA 0.2, ATP 3, and GTP 0.3) were directed to the selected neurons under visual control. In some recordings (Fig. 4*A–D*), a Cs^+-based internal solution (in mM, NaCl 1, $MgCl_2$ 1, TEA-Cl 11, $CsCH_3SO_4$ 79, Hepes 10, EGTA 5, ATP 3, and GTP 0.3) was used. The data in Fig. 4*E* were recorded using this solution with 1 mM EGTA. For morphological reconstructions, 200 μM Alexa-488 or Alexa-555 (Molecular Probes) were added to the recording pipette solution. To avoid any ambiguity, only two cells (one color each) were subjected to staining attempts in each bulb. The slices were fixed in 4% paraformaldehyde (Sigma) for 2 h and rinsed. The bulbs were then excised and mounted in 85% glycerol. The cells' morphology was reconstructed by taking confocal 3D stacks.

Data Analysis. Image analysis was performed using custom programs written in MATLAB (MathWorks). Regions of interest (ROI) corresponding to cell somata were selected using a semiautomatic algorithm and the average fluorescence intensities of individual ROIs were measured as a function of time. The background of each ROI was determined using a pixel-based algorithm (37) and subtracted before the calculation of $\Delta F/F$ values.

To identify synchronous M/T cells, fluorescence images were recorded over 180 s in the absence of stimulation. Slow baseline drifts of every trace (calculated by smoothing the trace with a Hanning filter, window length 8 s) were first subtracted from each trace (38). The activity correlation index (r) was defined as the zero-lag cross-correlation value between pairs of baseline-subtracted traces.

Data values are reported as mean ± SEM unless otherwise noted.

ACKNOWLEDGMENTS. We thank Drs. F. Wolf, W. Stühmer, E. Neher, and S.C. Lin for discussions, H. Schultens for very helpful comments on the manuscript, W. Mesecke, T. Nägel, and J. Kowalski for excellent technical help. The work was supported by the DFG Center for Molecular Physiology of the Brain, Excellence Cluster Grant EXC 171, Bernstein Center for Computational Neuroscience, the Göttingen Neuroscience Graduate School, and Carl Zeiss MicroImaging.

1. Mombaerts P, *et al.* (1996) Visualizing an olfactory sensory map. *Cell* 87:675–686.
2. Mori K, Nagao H, Yoshihara Y (1999) The olfactory bulb: coding and processing of odor molecule information. *Science* 286:711–715.
3. Shepherd GM, Greer CA (1998) in *Synaptic Organization of the Brain*, ed Shepherd GM (Oxford Univ. Press, New York, NY).
4. Isaacson JS, Strowbridge BW (1998) Olfactory reciprocal synapses: dendritic signaling in the CNS. *Neuron* 20:749–761.
5. Chen WR, Xiong W, Shepherd GM (2000) Analysis of relations between NMDA receptors and GABA release at olfactory bulb reciprocal synapses. *Neuron* 25:625–633.
6. Price JL, Powell TP (1970) An electron-microscopic study of the termination of the afferent fibres to the olfactory bulb from the cerebral hemisphere. *J Cell Sci* 7:157–187.
7. Jahr CE, Nicoll RA (1982) Noradrenergic modulation of dendrodendritic inhibition in the olfactory bulb. *Nature* 297:227–229.
8. Urban NN, Sakmann B (2002) Reciprocal intraglomerular excitation and intra- and interglomerular lateral inhibition between mouse olfactory bulb mitral cells. *J Physiol* 542:355–367.
9. Schoppa NE, Westbrook GL (2002) AMPA autoreceptors drive correlated spiking in olfactory bulb glomeruli. *Nat Neurosci* 5:1194–1202.
10. Pimentel DO, Margrie TW (2008) Glutamatergic transmission and plasticity between olfactory bulb mitral cells. *J Physiol* 586:2107–2119.
11. Christie JM, Bark C, Hormuzdi SG, Helbig I, Monyer H, Westbrook GL (2005) Connexin36 mediates spike synchrony in olfactory bulb glomeruli. *Neuron* 46:761–772.
12. Migliore M, Hines ML, Shepherd GM (2005) The role of distal dendritic gap junctions in synchronization of mitral cell axonal output. *J Comput Neurosci* 18:151–161.
13. Cinelli AR, Hamilton KA, Kauer JS (1995) Salamander olfactory bulb neuronal activity observed by video rate, voltage-sensitive dye imaging. III. Spatial and temporal properties of responses evoked by odorant stimulation *J Neurophysiol* 73:2053–2071.
14. Friedrich RW, Laurent G (2001) Dynamic optimization of odor representations by slow temporal patterning of mitral cell activity. *Science* 291:889–894.
15. Yaksi E, Judkewitz B, Friedrich RW (2007) Topological Reorganization of Odor Representations in the Olfactory Bulb. *PLoS Biol* 5:e178.
16. Manzini I, Rossler W, Schild D (2002) cAMP-independent responses of olfactory neurons in Xenopus laevis tadpoles and their projection onto olfactory bulb neurons. *J Physiol* 545:475–484.
17. Nezlin LP, Heermann S, Schild D, Rossler W (2003) Organization of glomeruli in the main olfactory bulb of Xenopus laevis tadpoles. *J Comp Neurol* 464:257–268.
18. Lin BJ, Chen TW, Schild D (2007) Cell type-specific relationships between spiking and $[Ca^{2+}]_i$ in neurons of the Xenopus tadpole olfactory bulb. *J Physiol* 582:163–175.
19. Alonso JM, Usrey WM, Reid RC (1996) Precisely correlated firing in cells of the lateral geniculate nucleus. *Nature* 383:815–819.
20. Cobb SR, Buhl EH, Halasy K, Paulsen O, Somogyi P (1995) Synchronization of neuronal activity in hippocampus by individual GABAergic interneurons *Nature* 378:75–78.
21. Schoppa NE (2006) Synchronization of olfactory bulb mitral cells by precisely timed inhibitory inputs. *Neuron* 49:271–283.
22. Gibson JR, Beierlein M, Connors BW (1999) Two networks of electrically coupled inhibitory neurons in neocortex. *Nature* 402:75–79.
23. Hayar A, Shipley MT, Ennis M (2005) Olfactory bulb external tufted cells are synchronized by multiple intraglomerular mechanisms. *J Neurosci* 25:8197–8208.
24. Scheidweiler U, Nezlin L, Rabba J, Muller B, Schild D (2001) Slice culture of the olfactory bulb of Xenopus laevis tadpoles. *Chem Senses* 26:399–407.
25. Perkel DH, Gerstein GL, Moore GP (1967) Neuronal spike trains and stochastic point processes. II. Simultaneous spike trains *Biophys J* 7:419–440.
26. Reid RC, Alonso JM (1995) Specificity of monosynaptic connections from thalamus to visual cortex. *Nature* 378:281–284.
27. Carleton A, Petreanu LT, Lansford R, varez-Buylla A, Lledo PM (2003) Becoming a new neuron in the adult olfactory bulb. *Nat Neurosci* 6:507–518.
28. Carlson GC, Shipley MT, Keller A (2000) Long-lasting depolarizations in mitral cells of the rat olfactory bulb. *J Neurosci* 20:2011–2021.
29. Schoppa NE, Westbrook GL (2001) Glomerulus-specific synchronization of mitral cells in the olfactory bulb. *Neuron* 31:639–651.
30. Buonviso N, Chaput MA (1990) Response similarity to odors in olfactory bulb output cells presumed to be connected to the same glomerulus: electrophysiological study using simultaneous single-unit recordings. *J Neurophysiol* 63:447–454.
31. Luo M, Katz LC (2001) Response correlation maps of neurons in the mammalian olfactory bulb. *Neuron* 32:1165–1179.
32. Kauer JS (1974) Response patterns of amphibian olfactory bulb neurones to odour stimulation. *J Physiol* 243:695–715.
33. Egana JI, Aylwin ML, Maldonado PE (2005) Odor response properties of neighboring mitral/tufted cells in the rat olfactory bulb. *Neuroscience* 134:1069–1080.
34. Czesnik D, Rossler W, Kirchner F, Gennerich A, Schild D (2003) Neuronal representation of odourants in the olfactory bulb of *Xenopus laevis* tadpoles. *Eur J Neurosci* 17:113–118.
35. Laurent G (2002) Olfactory network dynamics and the coding of multidimensional signals. *Nat Rev Neurosci* 3:884–895.
36. Marin EC, Jefferis GS, Komiyama T, Zhu H, Luo L (2002) Representation of the glomerular olfactory map in the Drosophila brain. *Cell* 109:243–255.
37. Chen TW, Lin BJ, Brunner E, Schild D (2006) In situ background estimation in quantitative fluorescence imaging. *Biophys J* 90:2534–2547.
38. Cossart R, Aronov D, Yuste R (2003) Attractor dynamics of network UP states in the neocortex. *Nature* 423:283–288.